Meteorol. Atmos. Phys. 53, 33–49 (1994)

Meteorology and Atmospheric Physics

[1] Department of Marine, Earth and Atmospheric Sciences, North Carolina State University, North Corolina, U.S.A.
[2] Naval Research Laboratory, Washington, U.S.A.
[3] Centre for Atmospheric Sciences, Indian Institute of Technology, New Delhi, India

Monsoon Rainfall Simulations with the Kuo and Betts–Miller Schemes

K. Alapaty[1], S. Raman[1], R. V. Madala[2], and U. C. Mohanty[3]

With 14 Figures

Received March 23, 1993
Revised June 23, 1993

Summary

Two numerical experiments are performed using a nested grid regional model to study the performance of the Kuo and the Betts–Miller cumulus parameterization schemes in simulating the rainfall during an active monsoon period. Results indicate that the monsoon circulation features, such as the Somali jet and monsoon depression are better simulated with the Kuo scheme. With the Kuo scheme, predicted intensity and associated rainfall of the monsoon depression are in good agreement with the observations. Uncertainty in the adjustment parameters in the Betts–Miller scheme appears to have lead to the poor prediction of rainfall. Also, the Betts–Miller scheme showed considerable sensitivity to the convergence in the lower troposphere in the initial conditions over the Arabian Sea, leading to a prediction of a spurious intense tropical cyclone. This cyclone replaced the normal heat-low over the desert region. Rainfall distribution and its maximum along the west coast of India were predicted better with the Kuo scheme. Area-averaged convective heating rates indicated that the cumulus convection is deeper and more intense with the Kuo scheme. Also, area averaged evaporation rates far exceeded the rainfall rates with the Betts–Miller scheme while with the Kuo scheme these rates are in balance after the spinup period. Forecast errors in the zonally averaged specific humidities indicate that the model atmosphere is more humid with the Betts–Miller scheme.

1. Introduction

During the southwest monsoon season (June to September), Indian subcontinent and surrounding regions receive heavy rainfall. Monsoon depressions form over the Bay of Bengal as low pressure centers, develop into storms and some times into severe cyclonic storms giving rise to heavy rainfall over India. Also, west coast of India is one of the areas where heavy rainfall rates are observed very frequently. Lower level westerlies approach the Western Ghats almost at right angles after traveling thousands of kilometers over the warm Indian Ocean and the Arabian Sea giving rise to large rainfall rates. These mountains are located about 50 km inland, parallel to the west coast of India. Orographic lifting of the humid monsoon westerlies causes heavy rainfall over this region.

Several two dimensional analytical and numerical studies (e.g., Smith and Lin, 1983; Grossman and Durran, 1984; Ogura and Yoshizaki, 1988) indicate that the sensible and latent heat fluxes from the surrounding oceans, vertical wind shear, and Western Ghats play important roles on the rainfall rates along the west coast of India. Even though these studies gave some insight into the physical processes involved, they cannot simulate the observed spatial and temporal variation of rainfall. In order to simulate the observed rainfall rates more realistically, one needs a nonlinear three dimensional model. Such a model should have proper representation of dynamics, thermodynamics, topography and relevant physics. Physical processes associated with the monsoon

circulations should be realistically represented to simulate the observed spatial and temporal distribution of the rainfall. In addition, the model domain must be sufficiently large to simulate the synoptic-scale circulations.

Largescale and mesoscale weather prediction models use parameterization schemes to represent sub-grid scale cumulus convection processes. Detailed physical processes that occur during life cycle of convective clouds are side-stepped and hence only bulk effects are considered in cumulus parameterizations such as the Kuo scheme (Kuo 1965, 1974), Betts–Miller scheme (Betts, 1986), and other schemes. Perhaps, the most widely used cumulus convection scheme in several research and operational models is the Kuo scheme, because of its simplicity and dependency on the largescale dynamics. Also, over the past two decades choices of different values for moistening parameter (b) were widely studied (e.g., Anthes, 1977; Geleyn, 1985; Molinari, 1983; Das et al., 1988). In the context of long-range weather prediction, it was noticed that the choice of small (almost equal to zero) moistening parameter can cause unrealistic drying of the atmosphere.

Based on observations, a new convective adjustment scheme was proposed by Betts (1986). The deep convection in this scheme is similar to the other moist convective adjustment schemes except that it uses observed quasi-equilibrium thermodynamic profile as a reference state rather than a moist adiabat. Baik et al. (1990a, 1990b) showed that the Betts–Miller scheme can simulate different stages of an idealized tropical cyclone starting from a weak initial vortex. Their results indicated that the simulated idealized tropical cyclone is sensitive to the saturation pressure departure parameter. Junker and Hoke (1990) compared performances of the 1965 Kuo scheme and the Betts–Miller scheme in predicting rainfall during winter season over the southern United States with the National Meteorological Center (NMC) nested grid model. Though the Betts–Miller scheme gave favorable precipitation scores, it showed a tendency for the mid-latitude cyclones to over-deepen. Puri and Miller (1990) studied the sensitivity of the cumulus parameterization schemes to the structure of four tropical cyclones observed during the Australian Monsoon Experiment (AMEX). Their results showed better vertical consistency of atmospheric structures with the Betts–Miller scheme than with the Kuo scheme. Both the analyses and forecasts showed considerable sensitivity to the Betts–Miller scheme by generating more intense cyclonic systems as compared to the Kuo scheme.

The Betts–Miller scheme has been used in the past either to simulate observed tropical or mid-latitude cyclones with a coarse horizontal resolutions (> 80 km). The performance of the Betts–Miller scheme has not been studied for the monsoon region. This paper compares the performance of the Kuo and the Betts–Miller schemes in simulating monsoon rainfall and associated circulations using a three dimensional limited area nested grid model.

2. The Model

The Naval Research Laboratory and North Carolina State University (NRL/NCSU) nested grid model is used in the present study. It is a primitive equation model written in σ-coordinate system having a one-way interacting nested grid network. The σ-coordinate is defined by $\sigma = p/p_s$, where p is the level pressure and p_s the surface pressure. For further model details, readers are referred to Madala et al. (1987). Various physical processes that are included in the model are discussed below.

2.1 Physical Processes

The model physics includes latent heat, sensible heat, and momentum exchange between the atmospheric boundary layer and the underlying surface using the surface layer similarity theory (Businger et al., 1971), grid-scale precipitation, dry convection, and diffusion processes. Moist convective parameterization schemes used in the model are described in the next subsection. The short and long wave radiative processes are not included in the presence model. A second-order diffusion for momentum on σ-surfaces and for heat and water vapor on p-surfaces is used to account for the cascading of energy into unresolved subgrid-scale waves. If super-saturation exists at any level, the excess moisture is assumed to condense and fall out to the next lower layer and evaporate or continue to fall depending upon the degree of the saturation at that level. The model has a dry convective adjustment procedure to remove dry

convective instability that can occur during model integration.

2.2 Cumulus Parameterization Schemes

Two cumulus convection parameterization schemes are used in the model simulations. In the first simulation, the Kuo scheme is used. The moistening parameter b is calculated according to the method suggested by Anthes (1977) and is given by

$$b = [1 - \langle RH_g \rangle]^n, \quad (1)$$

where $\langle RH_g \rangle$ is the mean environmental relative humidity. We have used $n = 3$ for the moisture partitioning in the Eq. 1 consistent with the study on the convective heating rates over the monsoon region (Das et al., 1988). The Betts–Miller convective adjustment scheme assumes that in the presence of cumulus convection the local thermodynamic structures are constrained by the convection and adjusted towards observed quasi-equilibrium thermodynamic state. The Betts–Miller scheme contains shallow convection as well as deep convection. However, since the Kuo scheme deals with the deep convection, only the deep convection part of the Betts–Miller scheme is used for the comparative purpose. Adjustment parameters used in the Betts–Miller scheme are same as those used by Puri and Miller (1990) and Baik et al. (1990a). For further details, reader is referred to Betts (1986) and Baik et al. (1990a).

2.3 Numerical Method and Nesting Technique

The time integration scheme utilized in the present model is a split-explicit method which allows a larger time step by effectively separating various terms in the prognostic equations into parts governing slow-moving Rossby modes and fast-moving gravity modes. For the first and second fast-moving gravity modes smaller time step is used and for all other modes a larger time step is used. The implementation of these varying time steps is the basis for the split-explicit method. The time steps for the slow moving modes in the coarse-grid and the fine-grid domains are 300 s and 100 s, respectively, and appropriate smaller time steps satisfying CFL criterion are used for the fast-moving modes. For the horizontal differencing, a staggered grid network (Arakawa C-grid) is used with p_s, q, T, ϕ, $\dot{\sigma}$ specified at the same horizontal points, and u and v interlaced between them where p_s is the surface pressure, q the specific humidity, T the temperature, ϕ the geopotential, $\dot{\sigma}$ the vertical velocity, u the zonal wind velocity, and v is the meridional wind velocity. The finite difference technique used in the model is second-order accurate. It conserves total energy, mass, and momentum in the absence of the heat and momentum sources. In the model, the fine-grid mesh (FGM) overlaps one-third of the coarse-grid mesh (CGM) and the FGM is nested into the CGM such that every third grid point in the FGM is collocated with that in the CGM. The nested grid is positioned so that its boundary rows and columns overlap the CGM interior rows and columns. This nesting configuration enables the Fine-Grid Mesh domain boundary values to be specified by the Coarse-Grid Mesh interior grid points.

2.4 Data and Simulation Domain

Initial conditions are obtained from the European Center for Medium Range Weather Forecasts (ECMWF) analysis. Analyzed data are at 1.875° × 1.875° resolution at 14 vertical levels. Horizontal grid resolutions in the CGM and the FGM domains are 1.5° and 0.5°, respectively, and the vertical grid resolution in σ-coordinate is 0.1. Simulation domain is shown in the Fig. 1 and the CGM domain covers from 37.5° E to 112.5° E and

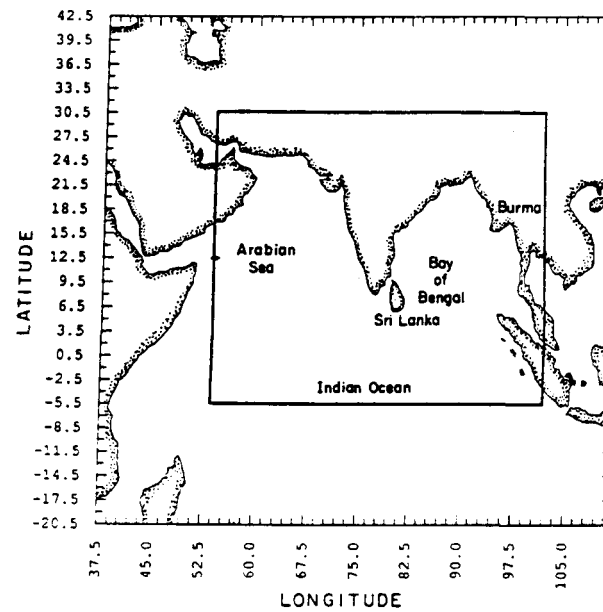

Fig. 1. The model domain of numerical simulation in the Coarse-Grid Mesh (CGM) and the Fine-Grid Mesh (FGM)

20.5° S to 42.5° N and the FGM domain from 54° E to 102° E and 5.5° S to 30.5° N. Model topography was obtained from the navy 10′ global topography data for 1.5° and 0.5° horizontal resolutions. Model sea surface temperatures (SST) were obtained from the 1° resolution global climatological values based on a 10 year average for the month of July. Davies scheme (1976, 1983) is employed to provide lateral boundary conditions using ECMWF analysis in the present version of the model. At the model top and bottom, the boundary for $\dot{\sigma}$ is zero.

2.5 *Numerical Experiments*

Two numerical simulations are performed for 48 hours starting at 12 UTC 16 July 1988. In the first experiment model simulations are performed with the Kuo scheme and in the second experiment with the Betts–Miller scheme. Coastline in both the CGM and the FGM domains are determined by the model topography data. Dark solid contours with bold zeros in all plots represent the model coastline.

2.6 *Synoptic Conditions*

Monsoon trough is one of the low-level features associated with the monsoon circulations. The orientation and its geographical location changes with the advancement of the monsoon. During the active monsoon period the monsoon trough has a northwest to southwest orientation with the western end located over northwest Rajasthan and the eastern end over the head Bay of Bengal. During such active monsoon periods, low pressure centers often develop over the bay of Bengal. These low pressure centers develop into monsoon depressions and some of these intensify into tropical cyclones giving rise to heavy rainfall over many parts of India. Due to the orographic lifting and associated convection, heavy rain occurs along the west coast of India. Also, the presence of a monsoon depression over Bay of Bengal can strengthen wind flow along the west coast of India leading to larger rainfall rates over this region.

Monsoon was active during the simulation period (12 UTC 16 July to 12 UTC 18 July) and large rainfall rates were observed. A monsoon depression was present over the Bay of Bengal close to the east coast of India. Analyzed streamline distribution and horizontal winds for the 850 hPa at 12 UTC 16 July 1988 (initial conditions) are shown in Fig. 2. Cyclonic circulation over the Bay of Bengal close to the east coast of India indicate the location of the monsoon depression. This depression moved northwest and made landfall during the next 24 h and later it moved further inland and was located over northeast India at 12 UTC 18 July. Large rainfall rates were reported over northeast India resulting from this monsoon depression. Along the west coast of India and offshore large rainfall rates are also observed. The low-level Somali Jet, also referred as to east

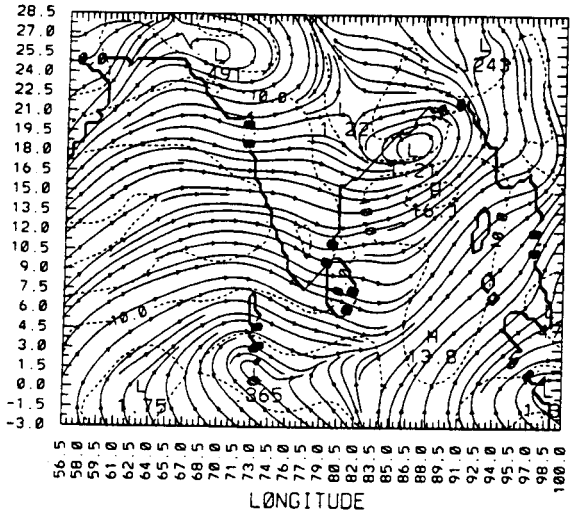

Fig. 2. Analyzed horizontal streamline and wind distribution at $\sigma = 0.85$ at 12 UTC 16 July 1988 (initial conditions). Contour interval is 5 m s^{-1}

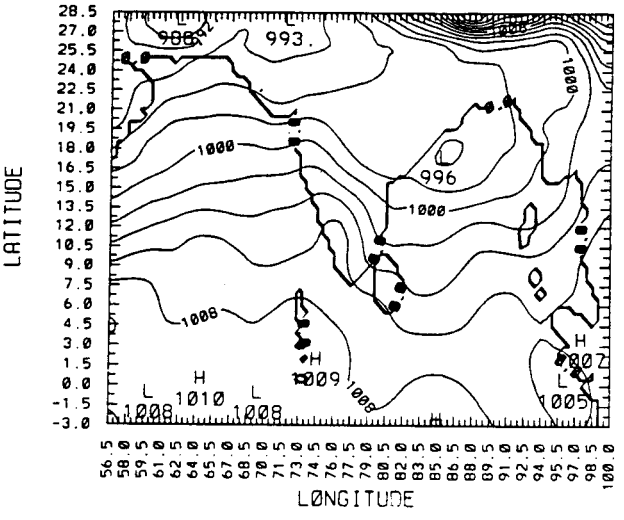

Fig. 3. Analyzed mean sea level pressure at 12 UTC 16 July 1988 (initial conditions). Contour interval is 2 hPa

African Jet, off the east coast of Africa is situated at a height of about 1.5 km from the surface. Strong winds (broken lines are isotachs) over the east coast of Africa are associated with the Somali jet over this region. The interaction of Somali jet with the monsoon circulation and its impact on the monsoon dynamics is still not well understood. analyzed mean sea level pressure at 12 UTC 16 July 1988 is shown in Fig. 3. The low pressure center off the east coast is the monsoon depression. Low pressure center over northwest India is due to the strong heating over the desert regions and is called the heat-low.

3. Discussion of Results

Model predictions using the Kuo and the Betts-Miller scheme are referred to as the KUO and the BMS, respectively. In this section, results from the KUO and the BMS are compared with the observations. Results from the coarse-grid model and fine-grid model are referred to as the CGM and the FGM, respectively.

3.1 Monsoon Circulation Features

At 12 UTC 16 July 1988 observed monsoon depression was located over the Bay of Bengal close to the east coast of India. During the next 24 h, monsoon depression made landfall and moved further inland in a northwesterly direction and at 12 UTC 18 July 1988 it was located over central India. Analyzed mean sea level pressure distribution for the FGM at 12 UTC 18 July 1988 is shown in Fig. 4a. Low pressure center over the central India indicates the location of the monsoon depression. Mean sea level (MSL) pressure distribution for the FGM at 48 h of simulation (12 UTC 18 July 1988) in the KUO and the BMS is shown in Fig. 4b and 4c, respectively. In the KUO, predicted location of the monsoon depression is about 3° south of the observed location and the orientation of the monsoon trough is similar to that of the observations (Fig. 4a). In the BMS, predicted monsoon depression is about 2° northeast of the observed location. Predicted trough is also northwest of the observed location. Comparing the MSL pressure at the center of the analyzed monsoon depression with that in the model predictions, it can be seen that the KUO predicted same value (993 hPa) as observed while the BMS pre-

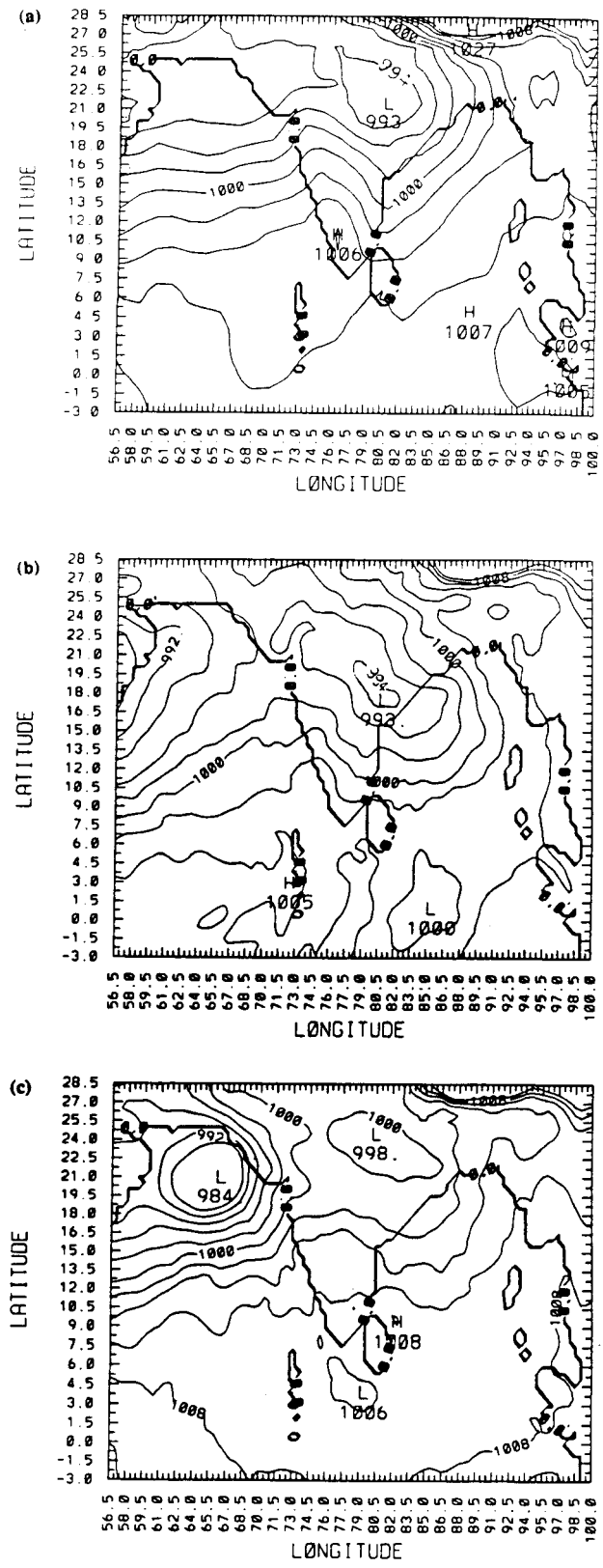

Fig. 4. Mean sea level pressure distribution for the FGM at 12 UTC 18 July 1988, from (a) analysis and from model predictions (b) in the KUO and (c) in the BMS. Contour interval is 2 hPa

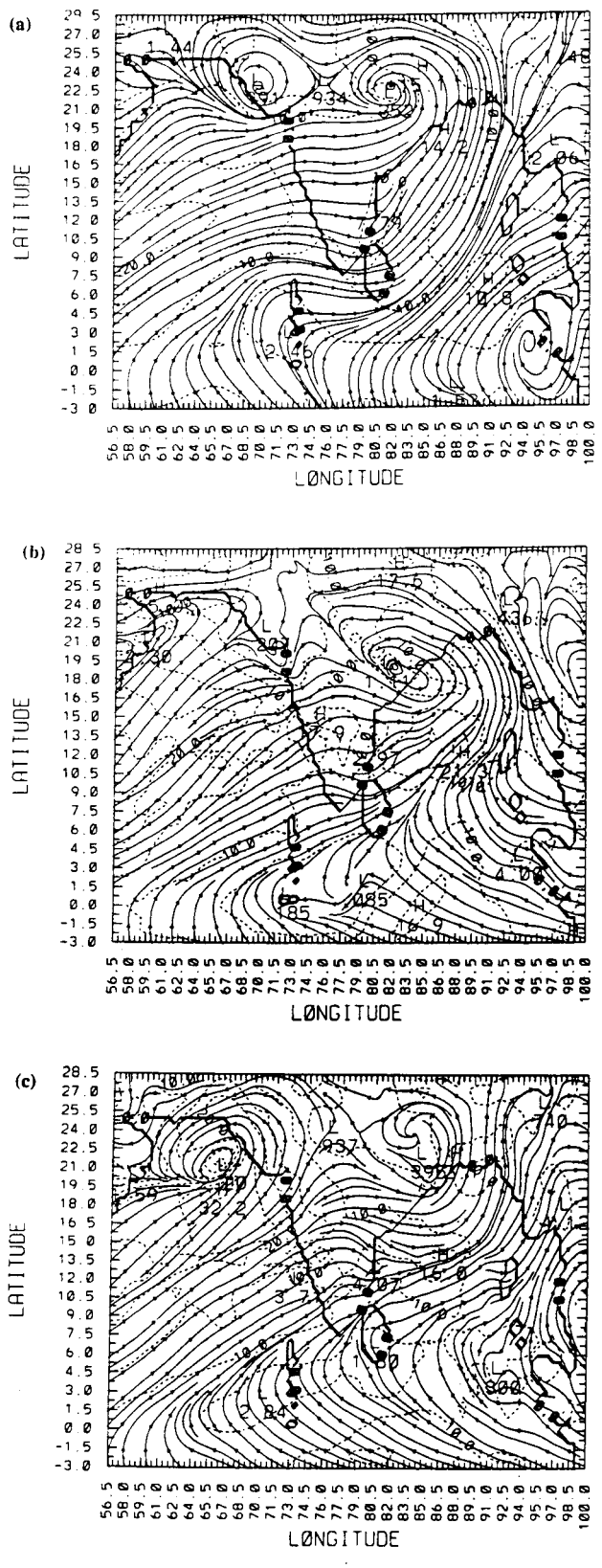

Fig. 5. Horizontal streamline and wind distribution at $\sigma = 0.85$ for the FGM at 12 UTC 18 July from (a) the analysis and from model predictions (b) in the KUO and (c) in the BMS. Contour interval is 5 m s^{-1}

dicted about 998 hPa. Thus, in the BMS, predicted monsoon depression is relatively weaker.

Mean sea level pressure distribution from the analysis (Fig. 4a) indicates that the heat-low is located over northwest India and the 994 hPa isoline indicates location of the heat-low (73° E, 24° N). Consistently, analyzed flow patterns in the lower levels indicates convergence (Fig. 5a) with cyclonic circulations over this region. In the KUO, mean sea level pressure distribution over the Arabian Sea is somewhat similar to that in the observations. Predicted pressure over the heat-low region is about 996 hPa, close to the observed value. On the other hand, mean sea level pressure distribution in BMS show different pattern. A superious low pressure system with cyclonic circulations is predicted over northern Arabian Sea. As indicated by the central pressure (984 hPa), this system is much stronger than the monsoon depression. This spurious system is a direct result of migration of the predicted heat-low to the Arabian sea in the BMS. Initially, (at 12 UTC 16 July 1988), observed heat-low was located northwest of India and during the next 48 h it had moved south to a location close to the west coast of India (73° E, 24° N). Convergence associated with this heat-low resulted in large evaporation and convective rainfall over this region (shown in a later section) leading to the intensification of the dislocated heat-low. As mentioned, predicted heat-low has become a spurious tropical cyclone, as indicated by its central pressure, winds and associated rainfall. This is further discussed in conjunction with the predicted rainfall in a later section.

Analyzed horizontal streamline distribution at about 850 hPa for the FGM at 12 UTC 18 July is shown in Fig. 5a. Broken lines represent isotachs. As discussed above, cyclonic circulations over the central and the northwest India are due to the presence of a monsoon depression and the heat-low, respectively. Corresponding predicted horizontal stream line patterns in the KUO and the BMS are shown in Fig. 5b and 5c, respectively. Streamline patterns in analyzed data and model predictions are consistent with the respective mean sea level pressure distributions over the regions of monsoon depressions and the heat-low. In the KUO, the heat-low as indicated by cyclonic circulations is located just south of the observed location but still over land, consistent with the

analyzed data. In the BMS, heat-low is absent over the land.

As mentioned earlier, analyzed wind data (isotachs) show the presence of Somali jet, indicated by strong winds off the east coast of Africa (Fig. 5a). Predicted wind distributions in the KUO (Fig. 5b) and in the BMS (Fig. 5c) also show the presence of Somali jet over this region. In the BMS, prediction of spurious low pressure system over the Arabian Sea resulted in stronger winds, particularly over the southwest sector of the system. This is due to the fact that the flow direction south of this spurious low pressure system is in the same direction as the mean flow of the Somali jet. Spatial distribution of wind in the KUO and the BMS are somewhat comparable to that in the analyzed data in other regions. Results from the CGM predictions (not shown) are qualitatively similar to that in the FGM predictions except that the winds are relatively weaker. This is obviously due to the coarser horizontal resolution of the CGM.

In order to compare the predicted wind field of the entire monsoon region with the observations, the CGM model predictions are considered since it covers a larger domain. Latitude-height section of the observed zonally averaged zonal winds for the CGM at 12 UTC 18 July is shown in Fig. 6a. Low level wind maximum between 6.5° and 18.5° N indicates the observed location of the Somali jet. Usually this jet is located at about 1.5 km from

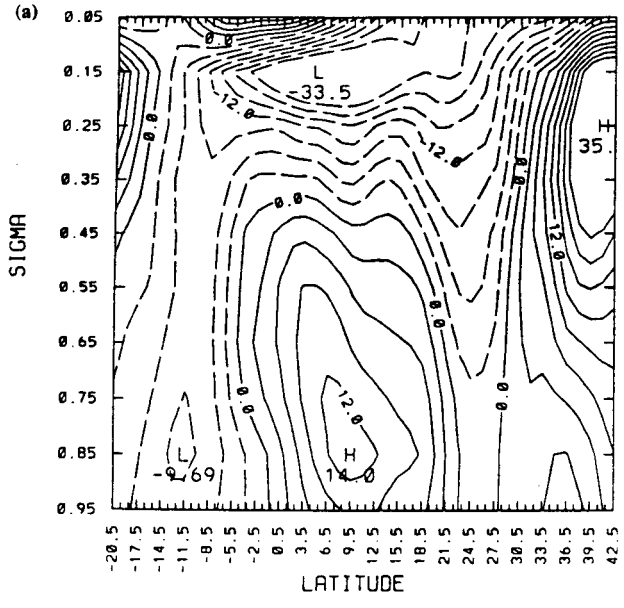

Fig. 6. (*Continued*)

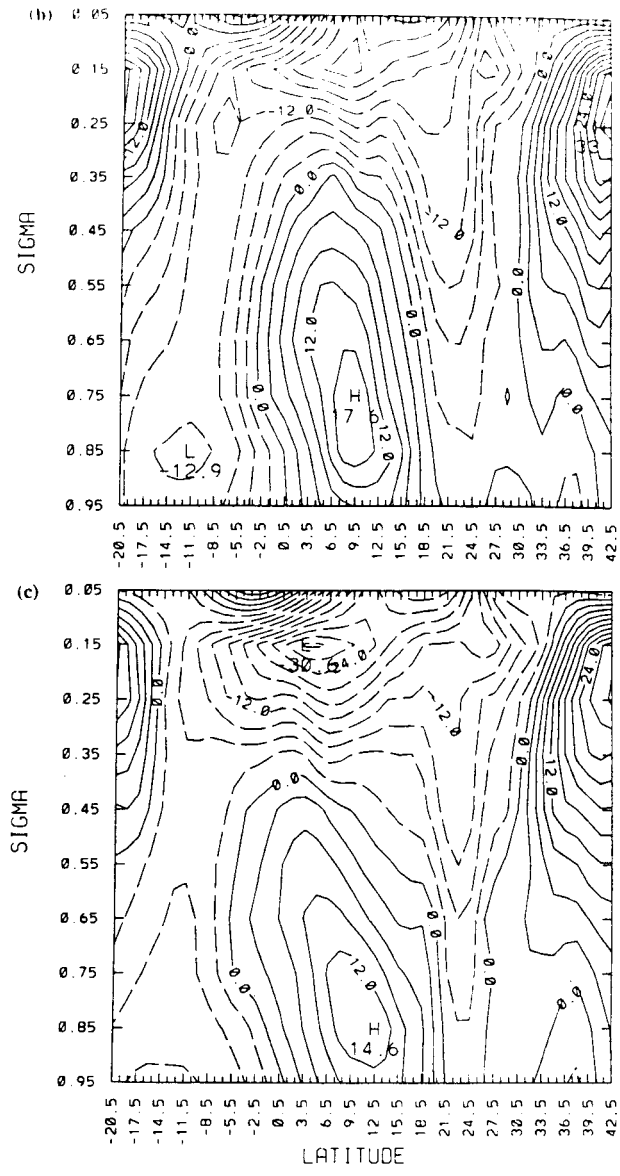

Fig. 6. Latitude-height section of zonally averaged zonal winds for the CGM at 12 UTC 18 July from (a) the analysis, and form the model predictions (b) in the KUO and (c) in the BMS. Contour interval is 3 m s^{-1}

the surface over the Arabian Sea, as can be seen in Fig. 6a. Wind maximum at upper levels (at $\sigma = 0.15$) is due to the presence of the Tropical Easterly Jet (TEJ). A strong vertical wind shear exists from the lower troposphere to the upper troposphere over this region. Wind maxima on the left and right side boundaries of Fig. 6a are due to the presence of subtropical westerly jets in the southern and the northern hemispheres, respectively. Corresponding latitudinally averaged zonal winds for the KUO and the BMS are shown

in Fig. 6b and 6c, respectively. In the KUO, predicted Somali jet is stronger than that in the BMS while the easterly jet is weaker in the KUO. Subtropical westerly jets over both the hemispheres are better simulated in the KUO while these jets are weaker in the BMS. In general, zonal winds are qualitatively similar in both the simulations.

Zonal average of analyzed meridional winds at 12 UTC 18 July for the CGM are shown in Fig. 7a. Meridional circulation north of equator indicates a reverse Hadley circulation with inflow at low levels and outflow at higher levels. During the summer monsoon season this kind of flow pattern is common over this region. Corresponding model predictions in the KUO and the BMS are shown in Fig. 7b and 7c, respectively. In both the forecasts, model predicts same intensity of the low level inflow up to a level of about 850 hPa. The upper level return flow (northerly component) is better simulated in the KUO although it is more intense than the observations. This indicates strong divergent flow at upper levels. The strong northerly flow in the upper levels is in conjunction with a strong southerly flow at lower levels. This in turn makes the westerly flow at lower levels somewhat weaker resulting in a weaker easterly jet.

3.2 *Water Vapor Budget*

Observations indicated that the monsoon was active during July 1988 with large rainfall rates

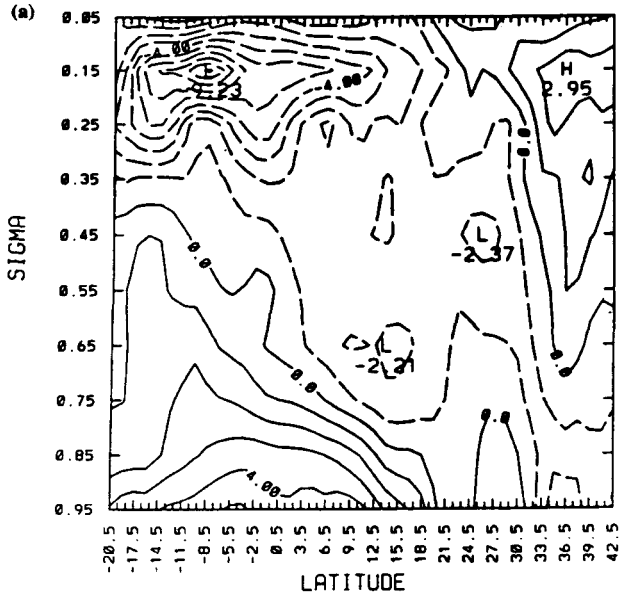

Fig. 7. (*Continued*)

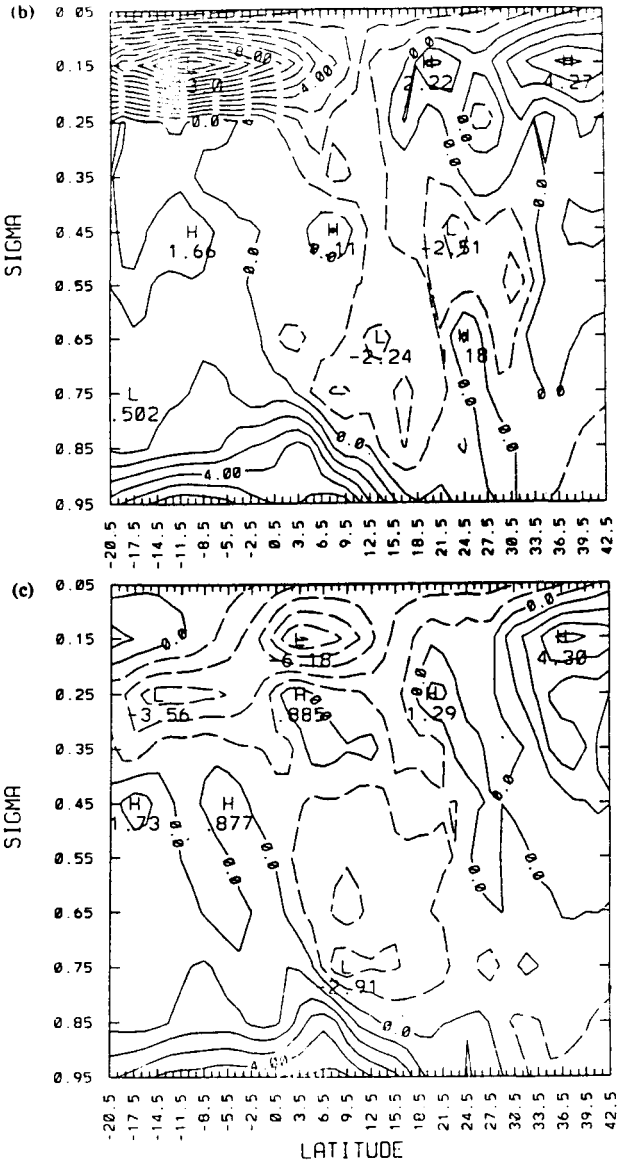

Fig. 7. Latitude-height section of zonally averaged meridional winds for the CGM at 12 UTC 18 July from (a) the analysis, and from the model predictions (b) in the KUO and (c) in the BMS. Contour interval is 1 m s^{-1}

(about 100 to 200 mm day^{-1}). Along the west coast of India observed rainfall is mainly due to the orographic-convective processes while over the central India it was due to the monsoon depression. During the period, 16 to 17 July 1988, the monsoon depression made landfall causing large rainfall rates of about 100 to 160 mm day^{-1} over central India (Fig. 8a). During the next 24 h, monsoon depression moved further northwest causing rainfall over this region (Fig. 8b). For these two days, observations (Fig. 8a and 8b) also

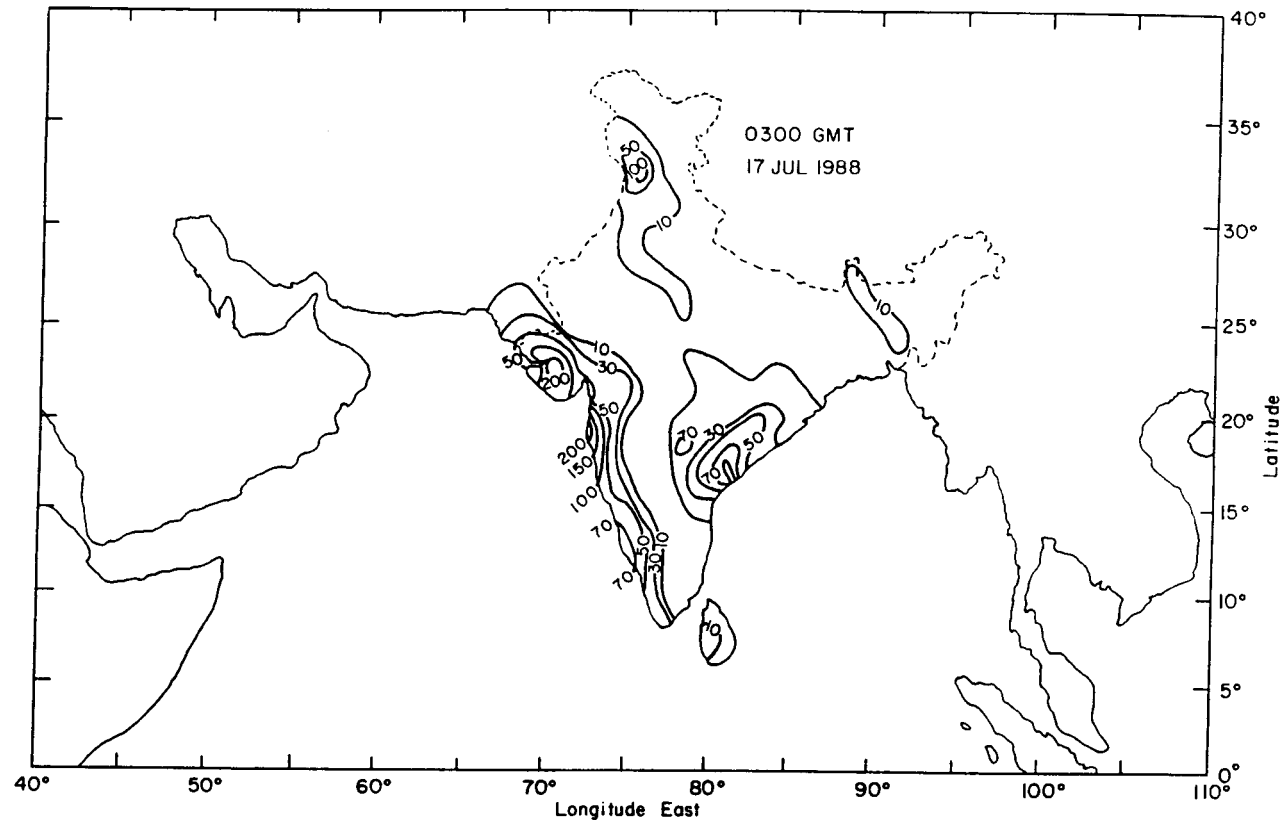

a

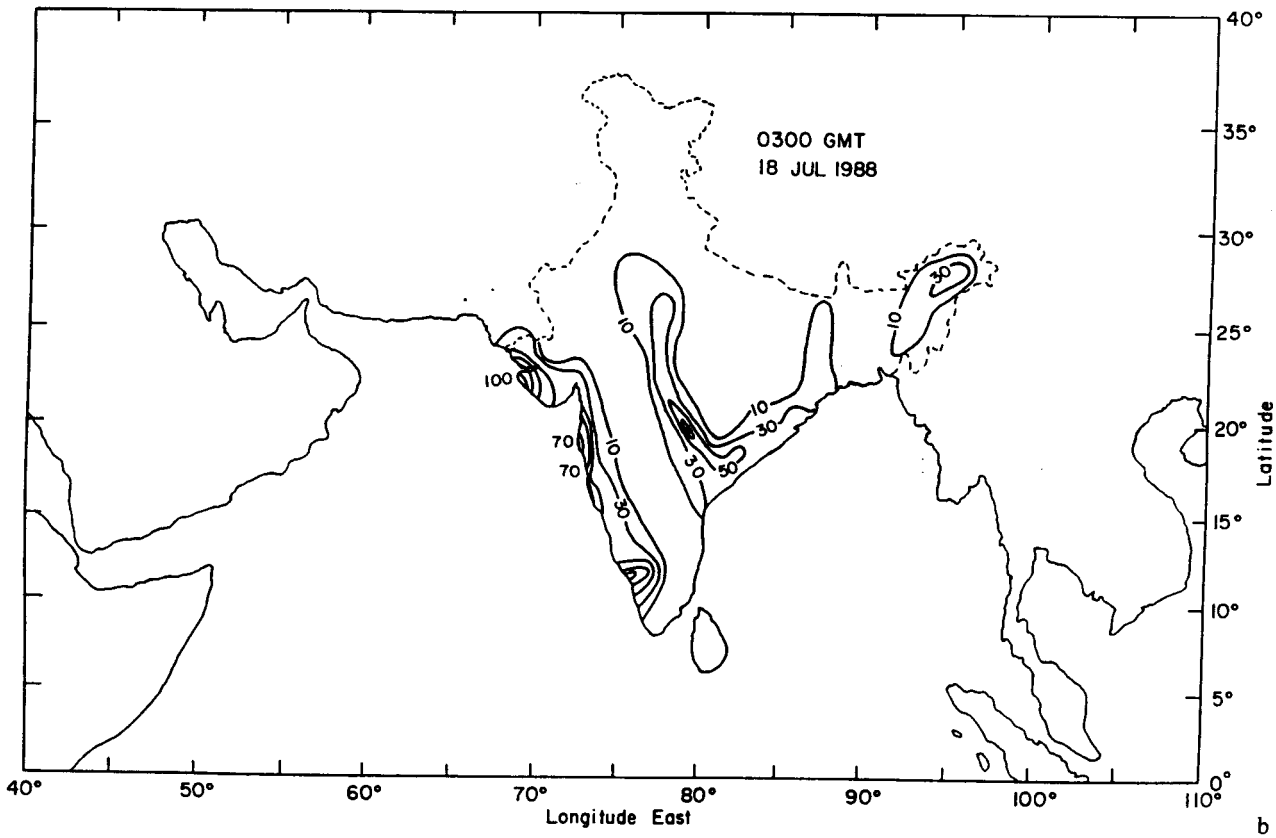

b

Fig. 8. Observed rainfall rates for a period of 24 hours (a) ending at 03 UTC 17 July 1988 and (b) 03 UTC 18 July 1988

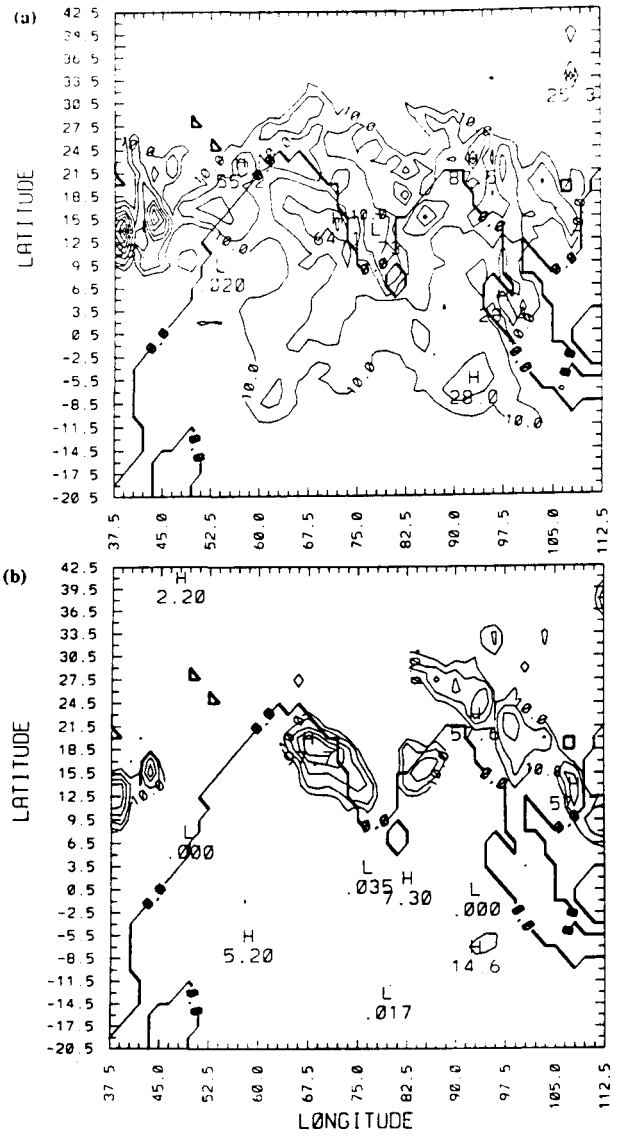

Fig. 9a, b. Predicted rainfall for the CGM domain for a period of 24 hours ending at 12 UTC 17 July 1988 in (a) the KUO and the (b) BMS, respectively. Contour intervals are 10, 20, 50, 80, 100, 125 mm d^{-1}

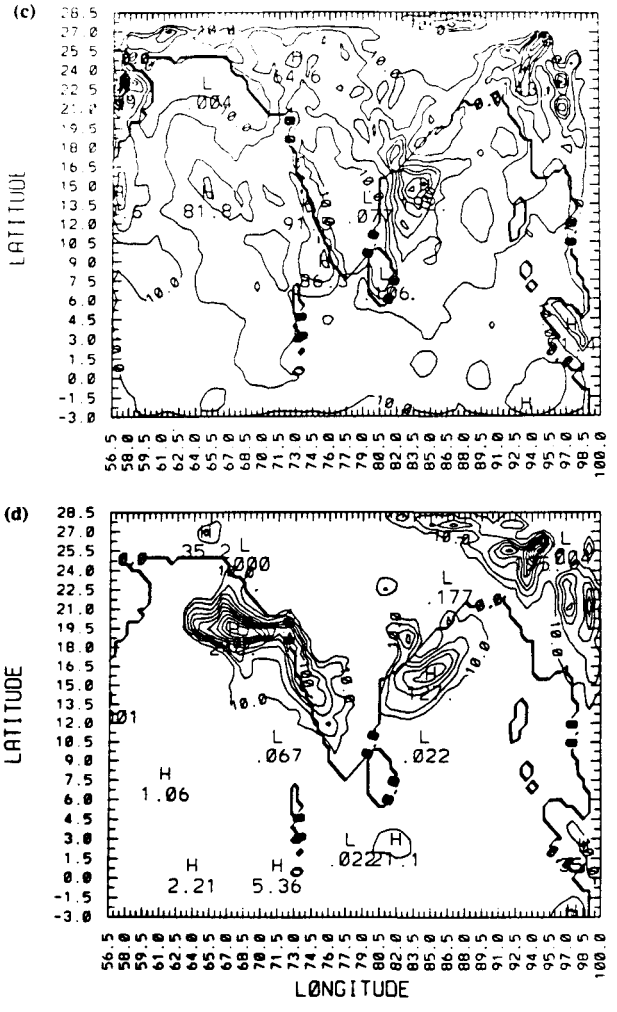

Fig. 9c, d. Predicted rainfall for the FGM domain for a period of 24 hours ending at 12 UTC 17 July 1988 in (c) the KUO and the (d) BMS, respectively. Contour intervals are 10, 25, 50, 75, 100, 125 mm d^{-1}

indicated rainfall rates of about 100–200 mm day^{-1} among the west coast of India. In general, there is an offshore extension of the rainfall over the Arabian sea (Ramakrishnan and Gopinatha Rao, 1958; Ramachandran, 1972). Krishnamurti et al. (1983) indicated that the location of the rainfall maximum during 1979 monsoon was just offshore. However, no observations are available offshore for this case study.

Predicted rainfall for the CGM ending at 12 UTC 17 July in the KUO and the BMS are shown in Figs. 9a and 9b, respectively. In both the forecasts model predicts more rainfall over the southwest sector of the monsoon depression. This is due to an increase in the low-level wind speed as the wind accelerated over the water and increased convergence caused by the movement of the depression relative to this low-level winds. Increase in low-level winds in the southwest sector of an offshore monsoon depression has been observed before (Rao, 1976). Spatial distribution of the rainfall over central India in the KUO is also consistent with the observed rainfall over that region. In the BMS, rainfall is limited to a small coastal region with none over the central India. Rainfall associated with the orography along the west coast of India is predicted by both the KUO and the BMS. In the KUO, rainfall maximum is located just

offshore of the west coast of India consistent with the generally observed pattern while in the BMS it is located over northern Arabian Sea, in conjunction with the spurios low. About 10 to 40 mm day^{-1} rainfall predicted over the Indian Ocean in the KUO. However, the BMS does not predict much rainfall over the Indian Ocean.

Predicted rainfall for the FGM ending at 12 UTC 17 July in the KUO and the BMS are shown in Figs. 9c and 9d, respectively. As expected, increased horizontal resolution in the FGM contributed to higher rainfall rates. Spatial distribution of rainfall associated with the model predicted monsoon depression for the FGM in the KUO is similar to that of the CGM but with higher rates ($\sim$ 192 mm day^{-1}). Predicted rainfall along the monsoon trough in the KUO is closer to the observations. In the BMS, rainfall maximum associated with the monsoon depression is only about 127 mm day^{-1}, less than that in the KUO. Also, in the BMS, predicted rainfall is confined to the east coast of India. Along the westcoast, about 91 mm day^{-1} rainfall was predicted in the KUO with maximum located just offshore. In the BMS, on the other hand, rainfall is predicted on the lee side of the Western Ghats as well as along the coast. However, largest rainfall rates (246 mm day^{-1}) are predicted over the northern Arabian

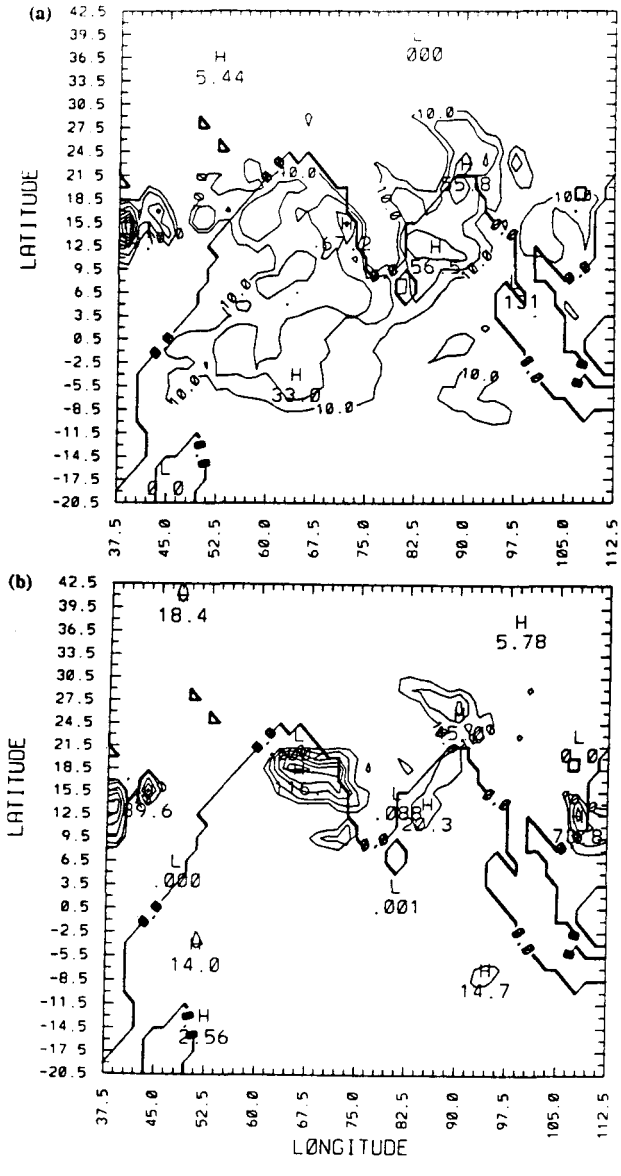

Fig. 10a, b. Predicted rainfall for the CGM domain for a period of 24 hours ending at 12 UTC 18 July 1988 in (a) the KUO and the (b) BMS, respectively. Contour intervals are 10, 20, 50, 80, 100, 125 mm d^{-1}

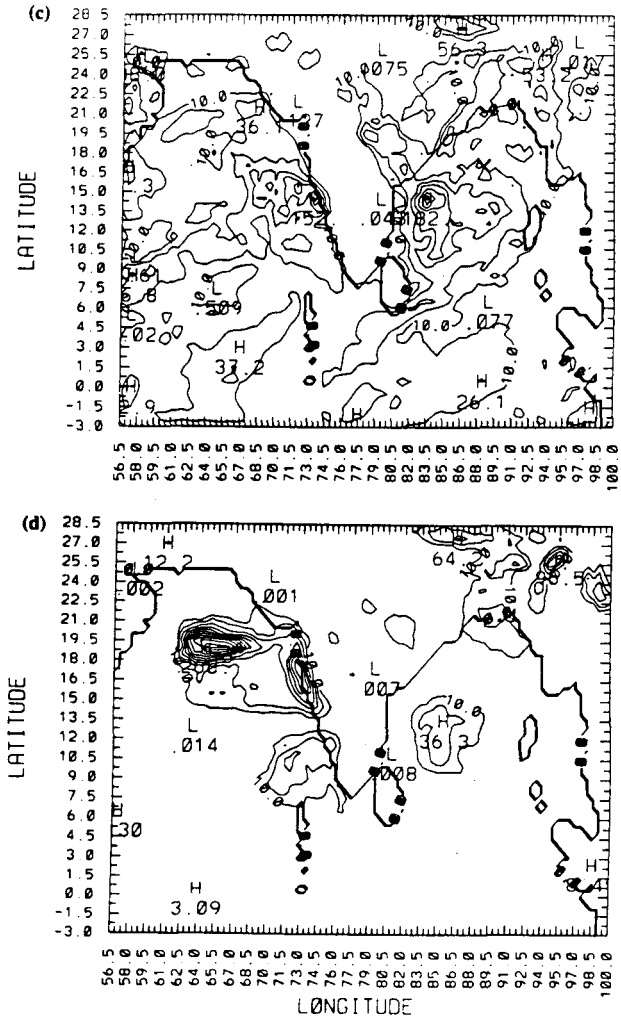

Fig. 10c, d. Predicted rainfall for the FGM domain for a period of 24 hours ending at 12 UTC 18 July 1988 in (c) the KUO and the (d) BMS, respectively. Contour intervals are 10, 25, 50, 75, 100, 125 mm d^{-1}

Sea in conjunction with the spurious low pressure system. Meager rainfall rates are predicted in the BMS over the Indian Ocean, indicating the some of the adjustment parameters such as saturation pressure departure, relaxation time scale and stability weights on the moist adiabat, used in the Betts–Miller scheme may not be suitable for the monsoon region.

Model predicted rainfall for the CGM during the second day of simulation ending at 12 UTC 18 July in the KUO and the BMS are shown in Figs. 10a and 10b, respectively. In the KUO, predicted rainfall along the monsoon trough region is smaller compared to the previous day. Along the west coast of India spatial distribution of rainfall is somewhat similar to that during the previous day. In the BMS, rainfall associated with the monsoon depression is very small as compared to that in the KUO. As mentioned earlier, predicted monsoon depression in the BMS has weakened during the second day as indicated by the rainfall predictions. On the other hand, spurious rainfall over the Arabian Sea in the BMS is larger as compared to that during the first day

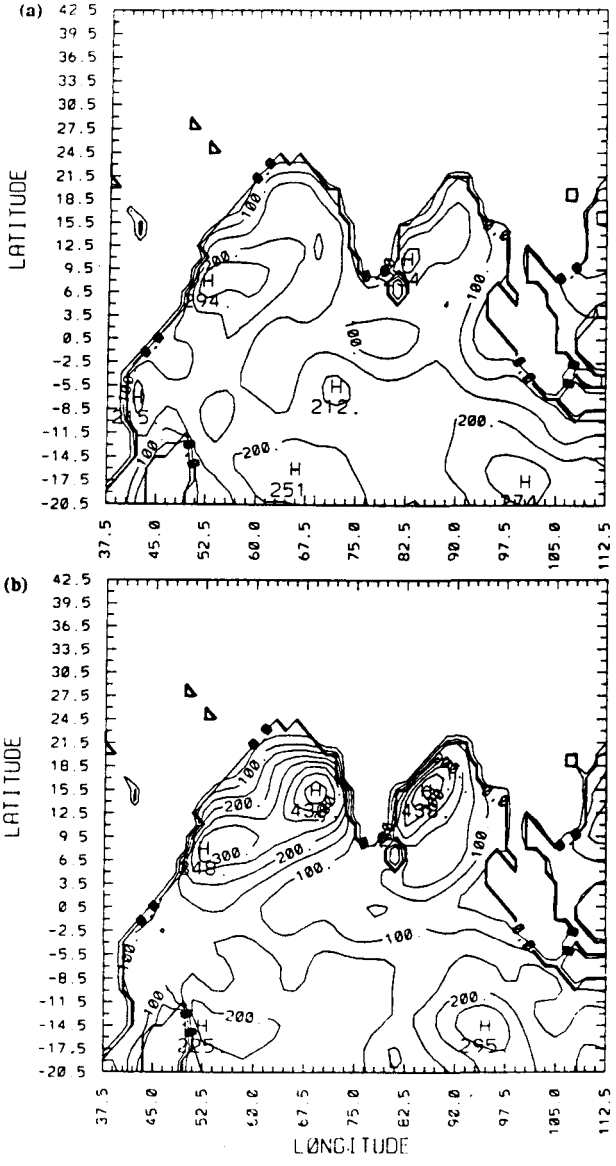

Fig. 11a, b. Mean latent heat fluxes from the surrounding oceans for 24 h ending at 12 UTC 17 July for the CGM (a) in the KUO and (b) the BMS. Contour interval is 50 W m^{-2}

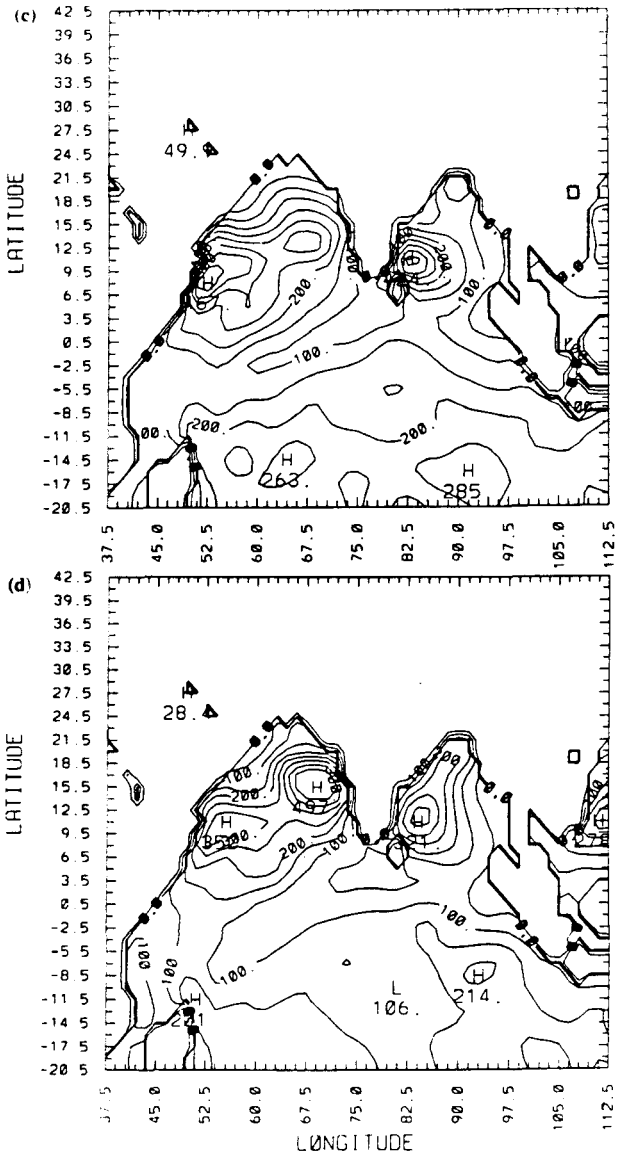

Fig. 11c, d. Mean latent heat fluxes from the surrounding oceans for 24 h ending at 12 UTC 18 July for the CGM (c) in the KUO and (d) the BMS. Contour interval is 50 W m^{-2}

of simulation. However, in the KUO, rainfall maximum just offshore of the west coast of India is again consistent with the observations.

Predicted rainfall for the FGM during the second day of simulation ending at 12 UTC 18 July in the KUO and the BMS are shown in Figs. 10c and 10d, respectively. As can be seen from the observations (Fig. 8b), a rainfall band along the monsoon trough region over central India is again well predicted in the KUO. In the BMS, rainfall over this region is again almost negligible ($10\,mm\,day^{-1}$). Again, over the surrounding oceans the BMS predicts lower rainfall rates as compared to that in the KUO. Along the west coast of India rainfall maximum predicted in the KUO is just offshore while in the BMS the spurious low pressure system has further intensified resulting in larger rainfall (about $268\,mm\,day^{-1}$).

The predicted rainfall should conform to the evaporation from the surrounding oceans. Daily average latent heat fluxes from the surrounding oceans for the first day of simulation for the coarse-grid mesh in the KUO and the BMS are shown in Figs. 11a and 11b, respectively. Since evaporation from the surface over land is not considered in the model, no latent heat fluxes exist over the land. Distribution of the latent heat fluxes in the KUO and the BMS are in good agreement with the climatological observations (Basu, 1990) off the Somali coast. Large latent heat fluxes in this region are caused by the presence of Somali Jet. But larger latent heat fluxes over the northern Arabian sea in the BMS are caused by the spurious storm and are not observed (Holt and Raman, 1985).

Daily average latent heat fluxes for second day of simulation for the CGM in the KUO and the BMS are shown in Figs. 11c and 11d, respectively. Off the Somali coast latent heat fluxes are larger in the KUO than that in the BMS. This is due to the intensification of the Somali jet in the KUO and stronger low level winds over this region. In general, latent heat fluxes of about 200 to $400\,W\,m^{-2}$ can be seen in both the KUO and the BMS forecasts. Again, the BMS predicts larger latent heat fluxes over northern Arabian sea. Over the Bay of Bengal (near the east coast of India), the spatial distribution of latent heat fluxes are similar.

3.3 Spinup and Forecast Errors

To determine the spinup time of the model, area average of rainfall for the entire CGM simulation domain is considered. Temporal variations of the area averaged rainfall and evaporation in the KUO and the BMS are shown in Fig. 12a. Solid line represents the hourly accumulated rainfall and dashed line represents the hourly accumulated evaporation in the KUO. In the BMS these fields are represented by respective lines with closed circles. Spinup signature can be seen in the KUO during the first day of simulation. After about 30 h of simulation the KUO shows good agreement between rainfall and the evaporation and there exists a balance between these two fields. In the

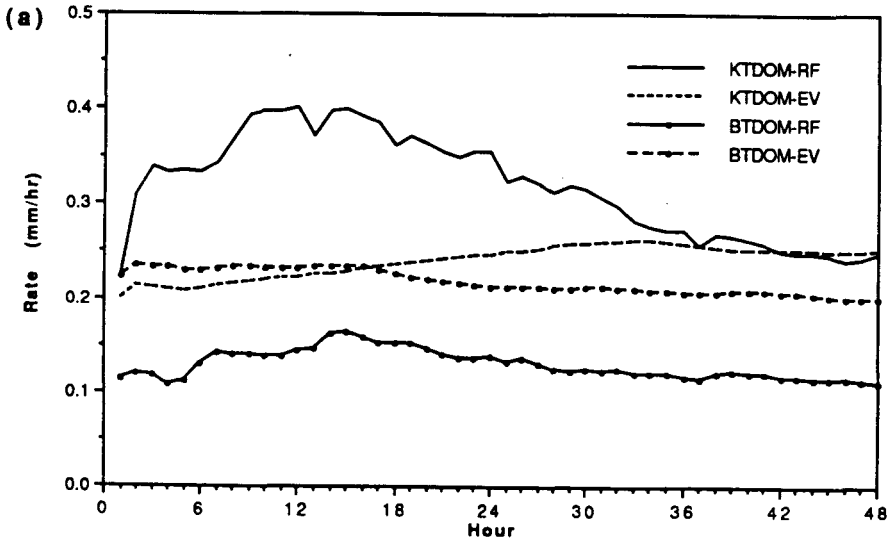

Fig. 12a. Temporal variation of hourly accumulated and area averaged (total domain) rainfall and evaporation in the KUO and the BMS

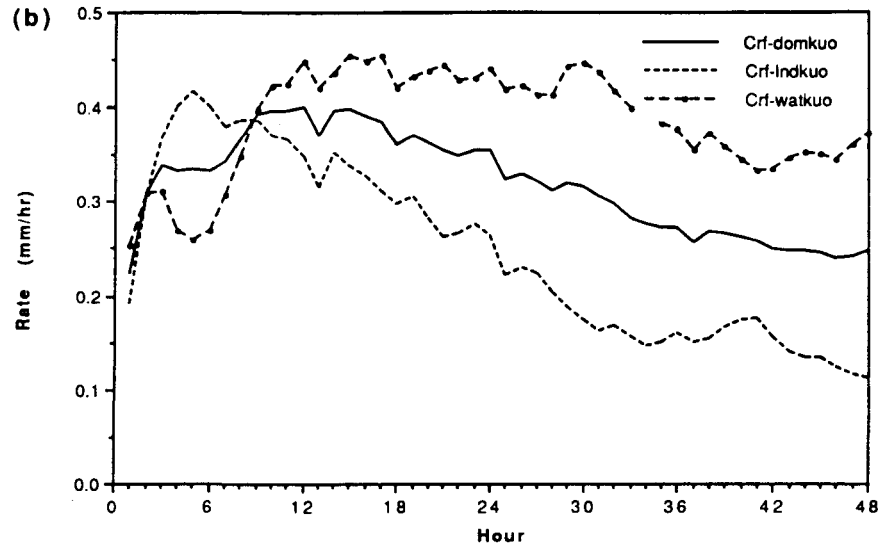

Fig. 12b. Temporal variation of hourly accumulated and area averaged rainfall (b) in the KUO for the entire domain (solid line), for the land-covered grid cells (dashed line) and for the water-covered grid cells (dashed line with closed circles)

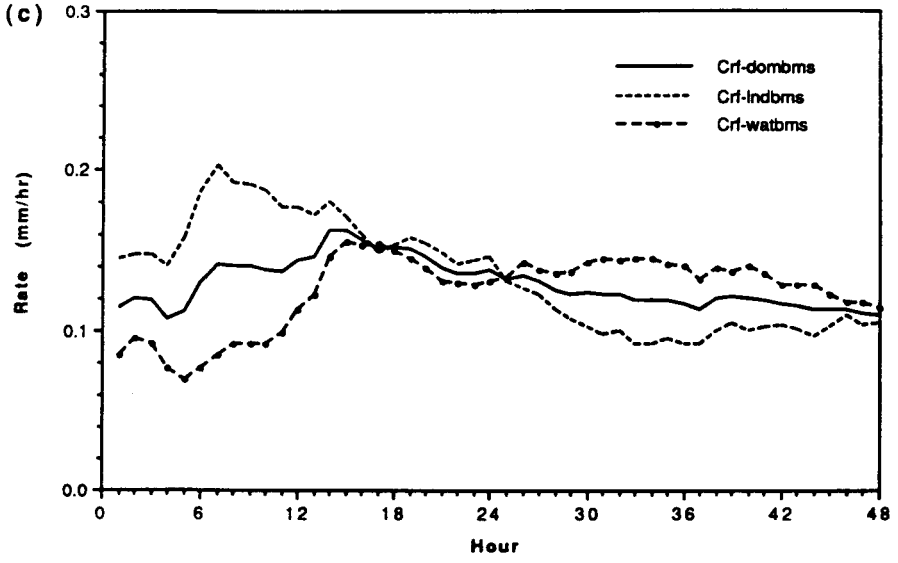

Fig. 12c. Temporal variation of hourly accumulated and area averaged rainfall (c) in the BMS for the entire domain (solid line), for the land-covered grid cells (dashed line) and for the water-covered grid cells (dashed line with closed circles)

BMS, accumulated rainfall is found to be underpredicted and shows a spinup time of about 18 h from the initial time. Up to 18 h of integration, model predicted similar rates of domain averaged evaporation for both the parameterization schemes. For the rest of the simulation model predicted higher evaporation rates with the BMS. This is due to the presence of spurious cyclone over the northern Arabian Sea. Winds are much more accelerated over the southern Arabian Sea, resulting in stronger southwesterlies over this region with the BMS. As a result, higher evaporation rates are predicted with the BMS. Evaporation in the BMS is found to be much higher than the rainfall though it showed a small decrease from first day to the second day. However, evaporation is found to be higher than the rainfall by about $0.1\,mm\,h^{-1}$. On the average, the KUO shows about $0.25\,mm\,h^{-1}$ of rainfall and evaporation rates whereas the BMS shows an average of about $0.1\,mm\,h^{-1}$. Thus, for the monsoon region after the spinup phase it is found that the rainfall predicted in the KUO is in better balance with evaporation as compared to that in the BMS.

In order to investigate the spinup problem, rainfall rates for the CGM over the land and over the ocean were separated. Temporal variations of hourly area averaged rainfall in the KUO for the entire domain (solid line), for the land-covered grid cells (dashed line) and for the water-covered grid cells (dashed line with closed circles) are shown in Fig. 12b. It is found that there is a spinup process for the model over both the land and the oceans for the first 12 h. Then the rainfall rate over

the oceans stabilized for the next 24 h. However, over land after 12 h, there is a continuous decrease in rainfall. Evaporation over land is not considered in the present version of the model and also the boundary layer processes are represented through bulk technique. These two factors might have contributed to the sharp decrease in the rainfall rates over the land.

Temporal variations of hourly area averaged rainfall in the BMS for the entire domain (solid line), for the land-covered grid cells (dashed line) and for the water-covered cells (dashed line with closed circles) are shown in Fig. 12c. Rainfall variation in this case indicates a spinup time of 16 h after which these rainfall rates are stabilized. During the first say of simulation rainfall rates over land are found to be higher than those over the oceans.

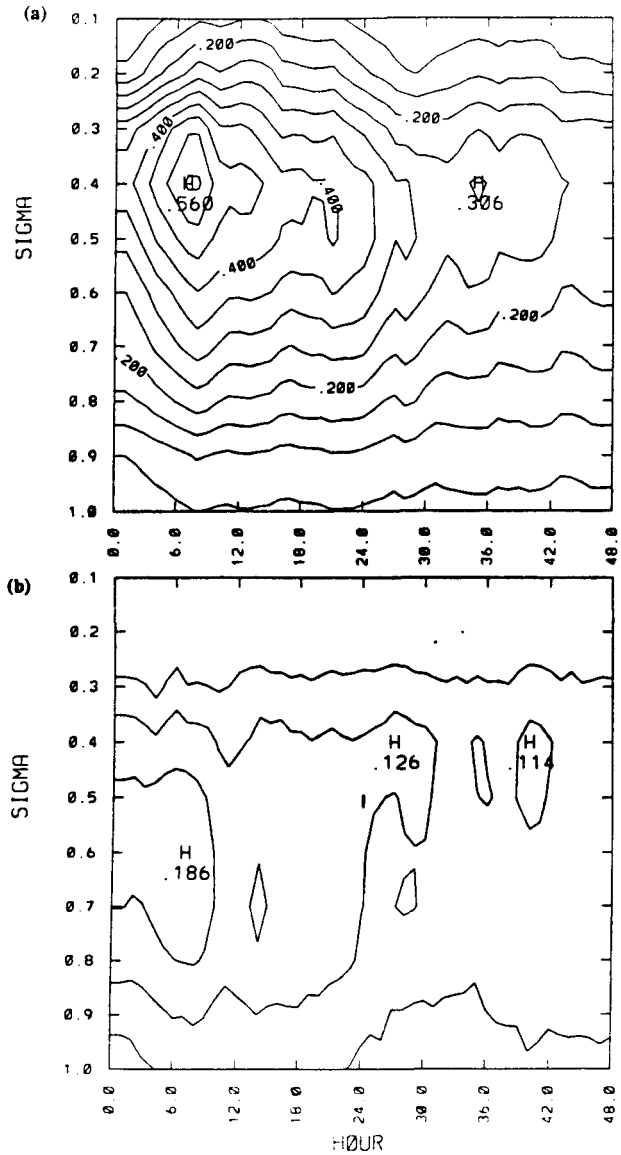

Fig. 13. Time-height section of the area averaged (total domain) convective heating for the FGM (a) in the KUO and (b) in the BMS. Contour interval is 0.05° K h^{-1}

In order to investigate the nature of the cumulus convection, area averaged (total domain) convective heating rates in the KUO and the BMS are considered. Time-height section of the area averaged convective heating rates for the FGM in the KUO and the BMS are shown in Figs. 13a and 13b, respectively. In the KUO, convective heating is found to be higher than in the BMS by about 0.2 to 0.4° K h^{-1} and maximum is located at about 400 hPa (0.4 σ). In the BMS, convective heating rates are smaller with an average heating of the atmosphere by about 0.15° K h^{-1}. In both the KUO and the BMS forecasts, convective heating maximum is present during early hours of integration as is reflected in the rainfall rates. Maximum convective heating in the KUO is located at about 400 hPa through out the simulation period. In the BMS, convection is rather shallow during the first day of simulation as compared to that in the KUO. Cumulus convection gradually deepend during the second day in the BMS, as indicated by the location of the maximum heating. Thus, more intense and deeper cumulus convection is found in the KUO as compared to that in the BMS.

To find out in the differences between the model predictions and the observations, latitudinal averages of atmospheric temperatures were considered. In the middle and upper troposphere the KUO indicated warming of the atmosphere while in the BMS warming was confined to only lower and middle troposphere. Also, warming of the atmosphere in the KUO was larger than that in the BMS. These features are consistent with the convective heating rates.

Forecast errors in the zonally averaged specific humidities for the CGM in the KUO and the BMS at 48 h are shown in Figs. 14a and 14b, respectively. Over the oceanic regions low level moistening in both the KUO and BMS is due to the evaporation from the surface. In the KUO, atmosphere above the boundary layer and the middle troposphere is drier. On the other hand, in the BMS atmosphere is more moist except for a thin layer between 850 and 750 hPa. This may be due to the fact that the cumulus convection is not deep and rainfall rates are smaller in the BMS. Dry atmosphere in the KUO is mainly due to the

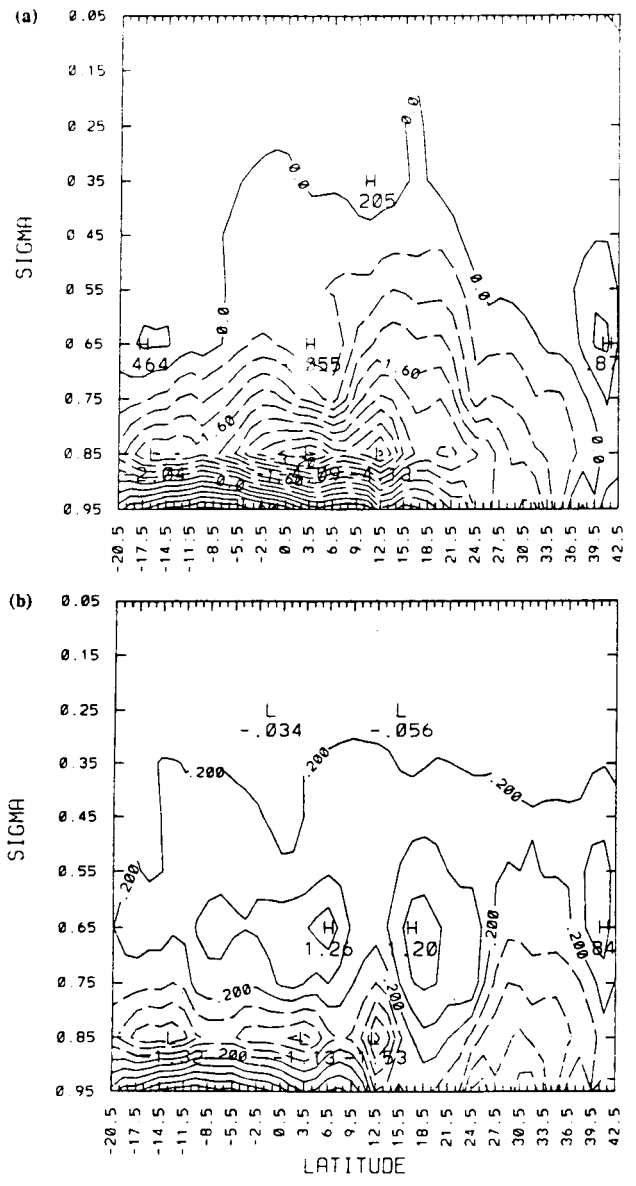

Fig. 14. Latitude-height section of zonal average of specific humidity differences between model predictions and the analyzed data (a) in the KUO and (b) in the BMS for the CGM at 12 UTC 18 July 1988. Contour interval is 0.4 gm Kg^{-1}

intense and deep convection resulting in large rainfall rates as compared to those in the BMS. Thus, both the temperature and the moisture fields are consistent with the convective processes in both the forecasts.

4. Conclusions

A ten-layer regional nested grid model is used to study the performance of two different cumulus parameterization schemes. Two numerical simulations are performed for 48 h starting at 12 UTC 16 July 1988 using the Kuo and the Betts–Miller schemes. Main features associated with the monsoon circulations such as the Somali jet, reverse Hadley cell, heat-low and monsoon depression are better predicted in the model simulations when the Kuo scheme is used. Predicted rainfall associated with the monsoon depression is in better agreement with the observations when the Kuo scheme is used. Surface pressure at the center of the monsoon depression and the location of the heat-low predicted with the Kuo scheme agree better with observations. Results indicate that the thermodynamic adjustment parameters used in the Betts–Miller scheme are very sensitive to the low-level cyclonic circulations over the Arabian sea. As a consequence, predicted heat-low moved south over the Arabian Sea and developed into an intense tropical cyclone when the Betts–Miller scheme is used.

Along the west coast of India, predicted rainfall rates due to the orographic lifting are lower compared to the observations with the Betts–Miller scheme. Comparison of area averaged rainfall indicated that the Kuo scheme yields more rainfall than the Betts–Miller scheme and evaporation predicted with the Betts–Miller scheme far exceed the predicted rainfall. Rainfall associated with the spurious storm over the Arabian Sea is also included in the area averaged rainfall rates and even with these large amounts domain averaged rainfall is lower compared to that with the Kuo scheme. In contrast, results from Australian Monsoon Experiment (Puri and Miller, 1990) indicate that the vertical structure and intensity of four tropical cyclones are better simulated with the Bettes–Miller scheme. In spite of the fact that the thermodynamic adjustment parameters used for the Betts–Miller scheme in this present study are very similar to those used by the Puri and Miller (1990), the conclusions in the present study on the overall performance of the Kuo and the Betts–Miller schemes differ significantly. However, results from this single case study indicate that the Betts–Miller scheme need systematic sensitivity studies regarding the suitability of the adjustment parameters for the monsoon region.

Comparison of the zonally averaged predicted specific humidities with the observations, indicated that the model atmosphere is more moist when Betts–Miller scheme is used, consistent with the

predicted rainfall amounts. Inclusion of evaporation from the land surface and longwave cooling of the atmosphere may improve the model predictions with the Kuo scheme. In general, model predictions with the Kuo scheme compared better with the observations. Our future research is to include more case studies and study the sensitivity of model predictions to different values of thermodynamics adjustment parameters such as saturation pressure departure, relaxation time scale and stability weights on the moist adiabat used in the Betts–Miller scheme.

Acknowledgements

This work was supported in part by the Naval Research Laboratory, Washington, D.C. and by the Division of International Program, National Science Foundation under grant INT-9008926. Computer resources were provided by the North Carolina Supercomputing Center, Research Triangle Park, NC.

References

Anthes, R. A., 1977: A cumulus parameterization scheme utilizing a one-dimensional cloud model. *Mon. Wea. Rev.*, **105**, 207–286.

Baik, J.-J., DeMaria, M., Raman, S., 1990a: Tropical cyclone simulations with the Betts convective adjustment scheme. Part I: Model description and control simulation. *Mon. Wea. Rev.*, **118**, 513–528.

Baik, J.-J., DeMaria, M., Raman, S., 1990b: Tropical cyclone simulations with the Betts convective adjustment scheme. Part II: Sensitivity experiments. *Mon. Wea. Rev.*, **118**, 529–541.

Basu, B. K., 1990: A study on air-sea fluxes over Indian sea. In: Sikka, D. R., Singh, S. S. (eds.) *Physical Processes in Atmospheric Models*. New York: Wiley Eastern Edition, 179–192.

Betts, A. K., 1986: A new convective adjustment scheme. Part I: Observational and theoretical basis. *Quart. J. Roy. Meteor. Soc.*, **112**, 677–691.

Businger, J. A., Wyngaard, J. C., Izumi, Y., Bradley, E. F., 1971: Flux-profile relationship in the atmospheric surface layer. *J. Atmos. Sci.*, **28**, 181–189.

Das, S., Mohanty, U. C., Sharma, O. P., 1988: Study of Kuo-type cumulus parameterizations during different epochs of the Asian summer monsoon. *Mon. Wea. Rev.*, **116**, 715–729.

Davies, H. C., 1976: A lateral boundary formulation for multi-level prediction models. *Quart. J. Roy. Meteor. Soc.*, **102**, 405–418.

Davies, H. C., 1983: Limitations of some common lateral boundary schemes used in regional NWP models. *Mon. Wea. Rev.*, **111**, 1002–1012.

Geleyn, J.-F., 1985: On a simple, parameter-free partition between moistening and precipitation in the Kuo scheme. *Mon. Wea. Rev.*, **113**, 405–407.

Grossman, R. L., Durran, D. R., 1984: Interaction of low-level flow with the western Ghat Mountains and offshore convection in the summer monsoon. *Mon. Wea. Rev.*, **112**, 652–672.

Holt, T., Raman, S., 1987: A study of mean boundary-layer structures over the Arabian sea and the Bay of Bengal during active and break monsoon periods. *Bound.-Layer Meteor.*, **38**, 73–94.

Junker, N. W., Hoke, J. E., 1990: An examination of nested grid model precipitation forecasts in the presence of modearate-to-strong low-level southerly inflow. *Wea. Forecasting*, **5**, 333–344.

Krishnamurti, T. N., Cocke, S., Pasch, R., Low-Nam, S., 1983: Precipitation estimates from rainguage and statellite observations: Summer MONEX. Department of Meteorology, Florida State University, 377 pp.

Kuo, H. L., 1965: On the intensification of tropical cyclones through latent heat release by cumulus convection. *J. Atmos. Sci.*, **22**, 40–63.

Kuo, H. L., 1974: Further studies of the parameterization of the influence of cumulus convection on large-scale flow. *J. Atmos. Sci.*, **31**, 1232–1240.

Madala, R. V., Chang, S. W., Mohanty, U. C., Madan, S. C., Paliwal, R. K., Sarin, V. B., Holt, T., Raman, S., 1987: Description of the Naval Research Laboratory limited area dynamical weather prediction model. NRL Memo. Rep., No. 5992, Naval Research Laboratory, Washington, D.C., 131 pp.

Molinari, J., 1983: A method for calculating the effects of deep cumulus convection in numerical models. *Mon. Wea. Wea.*, **110**, 1527–1534.

Ogura, Y., Yoshizaki, M., 1988: Numerical study of orographic-convective precipitation over the eastern Arabian Sea and the Ghat mountains during the summer monsoon. *J. Atmos. Sci.*, **45**, 2097–2122.

Puri, K., Miller, M. J., 1990: Sensitivity of ECMWF analyses-forecasts of tropical cyclones to cumulus parameterization. *Mon. Wea. Rev.*, **118**, 1709–1741.

Ramachandran, G., 1972: The role of orography on wind and rainfall distribution in and around a mountain gap: Observational study. *Indian J. Meteor. Geophys.*, **23**, 41–44.

Ramakrishnan, K. P., Gopinatha Rao, 1958: Some aspects of the nondepressional rain in peninsular India during the southwest monsoon. *Proc. Symp. on the Monsoon World*, Indian Meteorological Department.

Rao, Y. P., 1976: Southwest Monsoon. Meteorological Monograph, Synoptic Meteorology No. 1/1976, India Meteorological Department, India, 367 pp.

Smith, R. B., Lin, Y.-L., 1983: Orographic rain on the western Ghat. In: Reiter, E. R., Baozhen, Z., Youngfu, Q. (eds.) *Proc. First Sino-American Workshop on Mountain Meteorology*, pp 71–94.

Authors' addresses: K. Alapaty, S. Raman, Department of Marine, Earth and Atmospheric Sciences, North Carolina State University, N.C. 27695-8208, U.S.A.; R.V. Madala, Naval Research Laboratory, Washington, D.C., 20375, U.S.A.; U. C. Mohanty, Centre for Atmospheric Sciences, Indian Institute of Technology, New Delhi, 110016, India.